Pergamon

0017–9310(93)E0100–U

Entrainment and demixing in subsonic thermal plasma jets: comparison of measurements and predictions

J. R. FINCKE, C. H. CHANG, W. D. SWANK and D. C. HAGGARD

Idaho National Engineering Laboratory, EG&G Idaho, Inc., Idaho Falls, ID 83415, U.S.A.

Abstract—Measurements of velocity, temperature, entrained air, and Ar/He concentration profiles in a subsonic thermal plasma jet were obtained using an enthalpy probe and mass spectrometer combination. The rapid entrainment of air into the jet results in rapidly decreasing velocities and temperatures. A significant diffusive separation of the premixed Ar/He feed gases is observed in the large temperature gradients present. Predictions are obtained from a comprehensive computational model of the thermal plasma jet. The 2-D axisymmetric model includes self-consistent effective binary and ambipolar diffusion and uses a k–ε turbulence model.

INTRODUCTION

ENTRAINMENT of cold gas into turbulent, high temperature, and high velocity atmospheric pressure plasma jets dominates behavior [1]. Entrainment alters chemical composition and greatly influences velocity and temperature profiles. The entrainment process has been the subject of several recent investigations [2–5]. The evidence suggests that entrainment is more of an engulfment [1–4], rather than simple diffusion. The cold engulfed gas bubbles are rapidly transported toward the core of the jet by turbulence, quickly cooling and slowing the jet. Dissipation of these bubbles by molecular diffusion is a relatively slow process.

In addition to entrainment, the composition of the plasma can be altered by demixing of the plasma gases. Inside the torch very large temperature gradients and concentration gradients of both the neutral and charged particles exist. This results in thermal diffusion, normal mass diffusion, and ambipolar diffusion. Since diffusion rates depend on the characteristics of the constituents (mass, viscosity, ionization potential, etc.) the result is diffusive demixing of the gaseous species. The effect is well known in both high pressure and low pressure stationary discharges [6–13]. Near the torch exit we have observed the depletion of Ar in the core of Ar/He thermal plasma jets due to ambipolar diffusion in the discharge region.

In this paper we present experimental and computational results on entrainment and demixing in a subsonic, Ar/He mixture, thermal plasma jet flowing into stagnant laboratory air. Experimental results are obtained by enthalpy probe measurements. The enthalpy probe has been used in high temperature flow field research since the 1960s [14–17] and is currently enjoying wide application in thermal plasmas [18–23].

The integration of a differentially pumped quadrapole mass spectrometer system with the enthalpy probe allows for the accurate determination of species concentration. In addition to concentration measurements, flow field velocity and temperature are obtained. Results show rapid entrainment of external air and significant demixing of the Ar and He plasma gas. These demixing effects persist for some distance downstream in the jet flow and are slowly mixed out by jet turbulence.

Previous modeling efforts in multicomponent plasma jets [24, 25] have been limited to simple approximations of two-component mixture consisting of plasma gas and surrounding air. These models are incapable of treating interactions between chemical reactions as well as separation of plasma gases. These models neglect interactions between multiple chemical reactions which consist of the dissociation of molecular nitrogen and oxygen and ionization of atomic species. For example, ionization of argon is suppressed by the electrons produced by ionization of other species. Because ionization processes are highly energetic and strongly temperature dependent, such interaction effects are clearly important. In addition the diffusion process in a plasma is controlled by diffusion of each ionized and neutral species. Faulty results would be produced from a simple diffusion treatment of previous modeling studies, since it is based on the total elemental concentration. For example, demixing occurring in the region near the torch exit could not be predicted properly, as explained later.

Species diffusion in plasmas introduces additional difficulties which are not encountered in conventional numerical simulations of multicomponent flows. In plasmas, due to the local electric field between electrons and ions, electron diffusion is controlled by the

NOMENCLATURE

C_p	specific heat of cooling water [J kg^{-1} K^{-1}]		y	axial coordinate [m].
CA_2	effective throat area of the orifice [m^2]		**Greek symbols**	
h	enthalpy [J kg^{-1}]		γ	specific heat ratio
K	equilibrium constant		ε	dissipation of turbulent kinetic energy [m^2 s^{-3}]
k	turbulent kinetic energy [m^2 s^{-2}]		ρ	density [kg m^{-3}]
$\dot{m}$	mass flow rate [kg s^{-1}]		σ	standard deviation.
P	pressure [N m^{-2}]			
Pr_t	turbulent Prandtl number		**Subscripts**	
R	gas constant [J kg^{-1} K^{-1}]		1	probe entrance
R_i	inside radius of torch nozzle [m]		2	probe exit
R_o	outside radius of torch housing [m]		atm	atmospheric
Sc_t	turbulent Schmidt number		cw	cooling water
T	temperature [K]		g	gas sample
ΔT_{cw}	cooling water temperature rise [K]		max	maximum at inflow boundary
V	free stream velocity [m s^{-1}]		stag	stagnation.
v	axial velocity [m s^{-1}]			
x	radial coordinate [m]		**Other symbols**	
x^c_{Ar}	cold mole fraction of argon		[ ]	molar concentration [mol m^{-3}].

ion diffusion, preserving charge neutrality [26]. This ambipolar diffusion requires special treatment, since applying conventional diffusion formulation will result in a charge separation due to the large diffusion coefficient of light electrons. Textbook treatments of the ambipolar diffusion in single elemental plasmas have recently been extended to multicomponent plasmas [27], using a self-consistent effective binary diffusion approximation [28].

This multicomponent ambipolar diffusion logic has been implemented in a newly developed, comprehensive computational model, whose features also include transients; kinetic and equilibrium chemistry with arbitrary numbers of species and chemical reactions; ideal gas mixtures with temperature-dependent thermodynamic and transport properties; subgrid scale (SGS) or k-ε turbulence models; and a stochastic particle spray model with melting. The model is embodied in a new computer code LAVA [29]. To our knowledge, no other thermal plasma model of comparable capabilities currently exists. This computational model has been applied to simulate argon plasma jets discharging into air [30] and particle spraying in an Ar–He plasma jet [31]. In this paper results are presented from a numerical simulation of the demixing of plasma gases in an Ar–He plasma jet, which is a non-trivial application of our general multicomponent ambipolar diffusion and chemistry logic.

ENTHALPY PROBE

The enthalpy probe, its operation, and performance have been described elsewhere [22, 23] hence only a brief description will be given here. The probe, Fig. 1, is a water jacketed gas sampling and stagnation pressure probe from which the enthalpy, temperature, and velocity of a hot flowing gas can be derived once the composition is known. A schematic of the enthalpy probe system showing cooling water and gas sample flow paths appears in Fig. 2. The calorimetric method used to determine gas enthalpy and hence temperature depends heavily on a 'tare' measurement. Observations of the coolant temperature rise and flow rate are made while no gas flows through the inner diameter of the probe. Gas is then allowed to flow and the same coolant measurements are repeated, together with measurements of the gas flow rate through the probe and gas temperature at the probe exit. The enthalpy probe energy balance is given by

$$\dot{m}_g(h_{1g} - h_{2g}) = \dot{m}_{cw} C_p [(\Delta T_{cw})_{\text{gas flow}} - (\Delta T_{cw})_{\text{no gas flow}}].$$

$$(1)$$

From the measured gas sample flow rate $\dot{m}_g$ and probe exit enthalpy h_{2g} the unknown gas enthalpy h_{1g} is now uniquely determined. Given this enthalpy, along with the atmospheric pressure and the assumption of local thermodynamic equilibrium, the other thermodynamic properties and gas temperature are obtained.

The exit gas sample enthalpy is determined from the measured temperature, composition, and pressure and the gas sample flow rate is measured via a sonic orifice. The orifice is choked provided the ratio of downstream pressure to upstream pressure is greater than $(2/\gamma + 1)^{\gamma/\gamma - 1}$. Note that γ is dependent on composition of the gas. Provided this criterion is met the
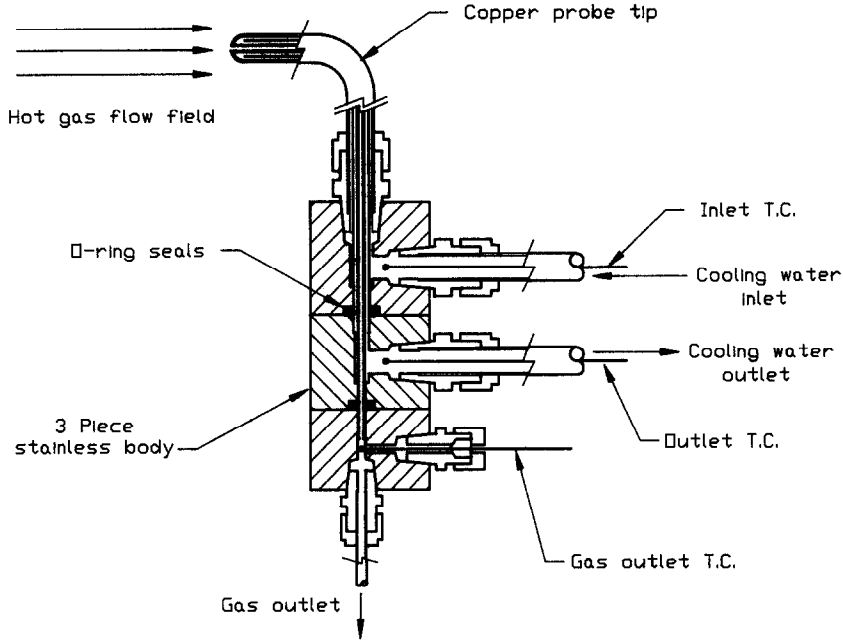
FIG. 1. Schematic of enthalpy probe.
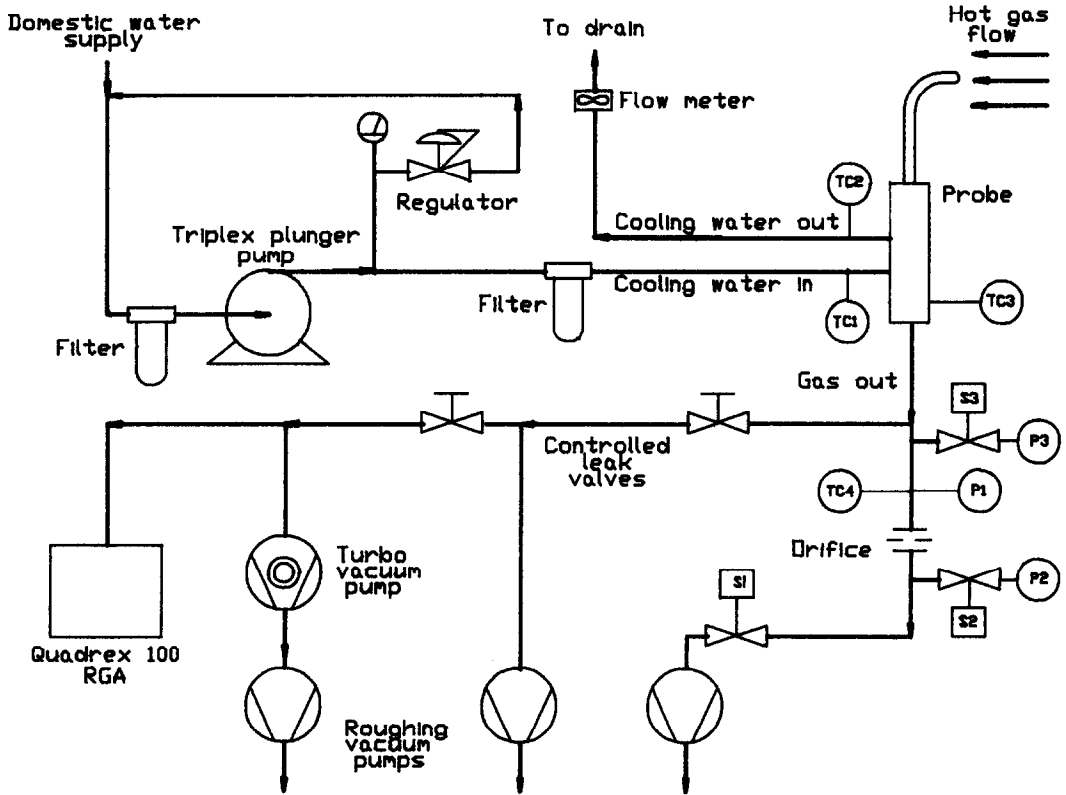

FIG. 2. Schematic of enthalpy probe system showing instrumentation in both cooling water and gas sample flow paths. S* = solenoid volume, P* = pressure transducer, and TC* = thermocouple.

mass flow rate through the orifice is a function of the upstream temperature and pressure,

$$\dot{m}_g = CA_2 P_1 \sqrt{\left(\frac{2}{R T_1}\right)\left[\frac{\gamma}{\gamma+1}\left(\frac{2}{\gamma+1}\right)^{2\gamma-1}\right]^{1/2}} \qquad (2)$$

where R is the composition dependent gas constant and CA_2, the effective throat area of the orifice, is determined by calibration against NIST traceable gas mass flow rate meters.

While the probe is in the 'no gas flow' mode of the measurement it behaves as a water cooled Pitot tube and the stagnation pressure is measured. For low Mach numbers, the free stream velocity, V, of the hot gas may be calculated from

$$V = \left[\frac{2}{\rho}(P_{stag} - P_{atm})\right]^{1/2} \qquad (3)$$

where ρ is the mixture density. The 2σ uncertainty in measured velocity and temperature is estimated to be 5.0 and 6.3%, respectively, at 1500 m s^{-1} and 12 500 K. The uncertainty in temperature increases to approximately 12% for temperature less than 6000 K. The velocity uncertainty is a 'percent of range' uncertainty. Therefore, the velocity is known to within ± 100 m s^{-1} everywhere in the flow field.

The probe itself is copper and has an outside diameter of 4.8 mm. The quadrapole mass spectrometer or residual gas analyzer (RGA) (Leybold-Heraeus Inficon Quadrex 100) samples the gas drawn through the probe. The RGA is set up in a differentially pumped vacuum system, Fig. 2. The sample line for the RGA is evacuated with a roughing pump to a pressure of approximately 1 torr. This pressure is regulated with a controlled leak at the probe and was chosen low enough for good response time but high enough to prevent preferential pumping of different sized molecules. A second controlled leak is located very close to the quadrapole sensor and is adjusted to maintain the pressure in the sensor vacuum system at approximately 10^{-6} torr. The limitations of the mass spectrometer and the largest source of error resides in the resolution of its 8 bit digitizer. This resolution error is minimized by optimizing the operating voltage of the electron multiplier and by adjusting the individual mass channel electronic gains until a reasonable sensitivity is achieved. Optimizing the gain in this way results in an uncertainty of 10% in the air fraction measurement, when the air fraction is in the neighborhood of 0.2. This uncertainty decreases with increasing air fraction. The uncertainty in the Ar/He ratio is also estimated to be approximately 10%. The system is calibrated using a known mixture of Ar, He, and air. Data acquisition, sample sequencing, and probe positioning, via a three-axis translation stage, is completely automated and computer controlled.
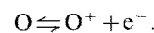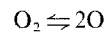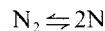
NUMERICAL SIMULATION

Numerical simulation has been performed to investigate the demixing processes using the LAVA code

[29]. Equations solved by LAVA consist of momentum and thermal internal energy equations for the multicomponent fluid mixture, continuity equations for each component of the mixture, and state relations for an ideal gas mixture with temperature-dependent specific heats and transport properties. Since detailed descriptions of the theoretical model and numerical scheme have been given elsewhere [29], only information regarding this simulation appears here.

Swirl effects are not included, since it is believed that the effects of swirl are negligible as reported in previous studies [4, 30]. Gravity has also been neglected. The plasma is assumed to be in the local thermodynamic equilibrium (LTE), which includes chemical equilibrium and thermal equilibrium, where electron temperature is the same as the heavy particle temperature.

Eleven species and six chemical reactions are considered in the calculation. The species considered are Ar, Ar$^-$, e$^-$, He, He$^+$, N$_2$, N, N$^+$, O$_2$, O, and O$^+$. Formation of NO$_x$ is neglected due to the negligible amount observed experimentally and the small amount of energy the reaction consumes. The chemical reactions are:

$$Ar \rightleftharpoons Ar^+ + e^-$$

$$He \rightleftharpoons He^+ + e^-$$

$$N_2 \rightleftharpoons 2N$$

$$O_2 \rightleftharpoons 2O$$

$$N \rightleftharpoons N^+ + e^-$$

$$O \rightleftharpoons O^+ + e^-.$$

These reactions are assumed to be in equilibrium.

Diffusion coefficients have been estimated from a simplified formula [30]. Viscosities and thermal conductivities of Ar–He–Air mixture are approximated by interpolating Ar–He properties and air properties as functions of temperature based on the local argon and helium mole fractions. Sophisticated mixture rules are not used, due to difficulties reported by Pateyron *et al.* [32] regarding Ar–He mixture plasmas and because turbulent transport is dominant. The radiation loss term was also approximated by the same interpolation between the corresponding terms for Ar–He mixture plasmas and air plasmas [33].

The effects of turbulence were modeled using the basic k–ε model described in previous studies [29, 30] with the same values of the various k–ε model constants of $Pr_t = Sc_t = 0.7$ instead of more conventional values of $Pr_t = Sc_t = 0.9$. The conventional k–ε model has particular difficulties in dealing with axisymmetric and swirling jets, for which ad hoc correction terms [34, 35] have been frequently employed. Effects of these correction terms for plasma jets have been studied previously [30], and none produced noticeably better results compared to the basic model. In the present simulation, we did not use any of the cor-
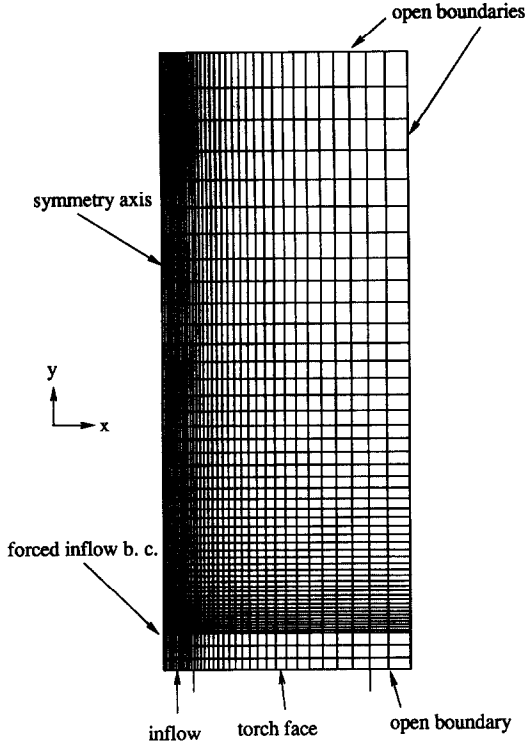
FIG. 3. Calculation domain and computational mesh.

rections to the basic k–ε model for axisymmetric jets [34] or swirling jets [35].

The computational domain is shown in Fig. 3. Torch geometry is taken from a commercial torch (Miller SG-100). The inside radius of the torch nozzle at the exit is $R_i = 4$ mm. The outside radius of the torch housing is $R_o = 33.3$ mm. The geometry is axisymmetric, so the simulation was performed in two-dimensional cylindrical coordinates. The calculational region is 4 cm radially by 10 cm axially, and is subdivided by a nonuniform 35×50 computational mesh as shown in Fig. 3. The radial coordinate is x and the axial coordinate is y. The left boundary is the symmetric axis, the bottom boundary is the nozzle exit plane, and the flow is upward. The torch face portion of the bottom boundary is treated as a solid wall. The remainder of the bottom boundary, as well as the top and right boundaries, are open boundaries at which the pressure is assumed to be ambient. The flow at these boundaries is calculated rather than imposed, so it can be either inward or outward at different locations on the boundary. Where inflow exists, the properties of the inflowing gas are taken to be those of the ambient air.

Inflow profiles of temperature and axial velocity are forced to match the experimental data at 5 mm from the nozzle exit (forced inflow b.c., Fig. 3), the closest available data to the nozzle exit. Radial velocities are assumed to be zero. In the region between the nozzle exit and 5 mm, the temperature and velocity are set to be the same as the experimental values at 5 mm.

The remainder of the bottom boundary not covered by experimental data is treated as explained above.

The integrated inflow rate of total energy is 10% less than that implied by the torch operating conditions. This difference is consistent with the experimental uncertainties in the velocity, enthalpy, and torch efficiency. Similarly, the mass inflow rate of Ar and He is overestimated by approximately 20%, also consistent with measurement uncertainties. The measurement of mass flow rate is subject to larger errors because a larger fraction of the mass flow is in the colder region of the jet, where the uncertainty in velocity measurements increases.

Local composition of ionized and dissociated species at the inflow is determined from the equilibrium conditions at the experimentally measured temperature and 'cold mole fraction' of argon, helium, and air. For example, the cold mole fraction of argon is given by

$$x_{\mathrm{Ar}}^{c} = \frac{[\mathrm{Ar}] + [\mathrm{Ar}^{+}]}{\begin{array}{c}[\mathrm{Ar}] + [\mathrm{Ar}^{+}] + [\mathrm{He}] + [\mathrm{He}^{+}] + [\mathrm{N}_2] \\ + [\mathrm{O}_2] + \frac{1}{2}([\mathrm{N}] + [\mathrm{N}^{+}] + [\mathrm{O}] + [\mathrm{O}^{+}])\end{array}} \tag{4}$$

where $[X]$ is the molar concentration of species X in the plasma. This is the argon mole fraction measured by sampling the plasma and cooling it to room temperature at constant elemental composition. Helium and air cold mole fractions can be represented by analogous expressions. These cold mole fractions uniquely determine the elemental composition fractions (i.e. atom fractions of Ar, He, N, and O). The molar concentrations of all species (Ar, Ar^{+}, e^{-}, He, He^{+}, N_2, N, N^{+}, O_2, O, and O^{+}) are then determined by solving the set of non-linear equations resulting from the assumption of chemical equilibrium. For example, the equilibrium condition for argon ionization is

$$K(T) = \frac{[\mathrm{Ar}^{+}]\,[\mathrm{e}^{-}]}{[\mathrm{Ar}]}. \tag{5}$$

These equations are solved iteratively using Newton's method. These equations actually determine only mole fraction ratios, from which absolute molar concentrations are obtained using the state equation $p = \Sigma_i \, c_i \, RT$ at the ambient pressure, where p and c_i represent pressure and molar concentration of species i, respectively.

Information regarding inflow profiles of turbulence cannot be obtained by the present experiments. We simply assumed the turbulent kinetic energy profiles at $y = 5$ mm as

$$k(x) = k_{\max} \left| \frac{\partial v}{\partial x} \middle/ \left(\frac{\partial v}{\partial x}\right)_{\max} \right| \tag{6}$$

where v is the axial velocity, $(\partial v/\partial x)_{\max}$ is the largest axial velocity gradient with respect to radial direction along the $y = 5$ mm line, and $k_{\max}$ is defined as

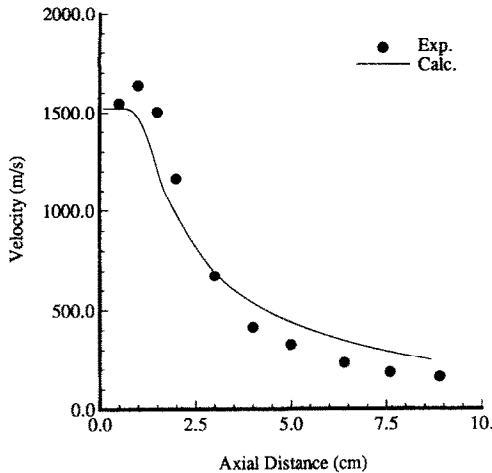FIG. 4. Calculated and experimental axial velocity along the centerline.

FIG. 5. Calculated and experimental radial profiles of axial velocity.

$$k_{max} = \tfrac{3}{2}(0.1v_{max})^2 \qquad (7)$$

and v_{max} is the largest inflow velocity. The inflow profile of ε was obtained from the turbulent kinetic energy profile by the prescription of Leschziner and Rodi [35].

The calculation was initialized by filling the calculation domain with quiescent ambient cold air, which is then displaced by, and mixes with, the incoming plasma until steady state is reached. The final steady solution is assumed to be unique and independent of the initial conditions and transient history [29].

RESULTS AND DISCUSSION

The plasma torch used is a commercial unit (Miller SG-100) operated with a standard anode and cathode combination (Miller *165 and *129, respectively). The torch has an 8 mm nozzle exit diameter and was operated at subsonic conditions. Torch operating conditions for the data presented are 800 A at 37 V, for a total power input of 29.6 kW. Approximately 67% of the input power is deposited in the torch gas. The argon and helium flow rates, including powder gas flow, were 3200 l h^{-1} and 1331 l h^{-1}, respectively, resulting in a mixture ratio [Ar]/[He] = 2.4. The ambient pressure is 85.5 kPa. Radial scans were made from -20 to $+20$ mm at regular intervals on the axis between 5 and 90 mm. The torch centerline is at 0 mm.

Calculated and experimentally obtained axial velocity and temperature are shown in Figs. 4–7. Calculated results show reasonable agreement with the experimental results except for the overly diffusive behavior near the torch exit. This behavior is consistent with the previous studies of plasma jets [30]. As explained in ref. [30], the results are expected to be improved by further studies in both turbulence model
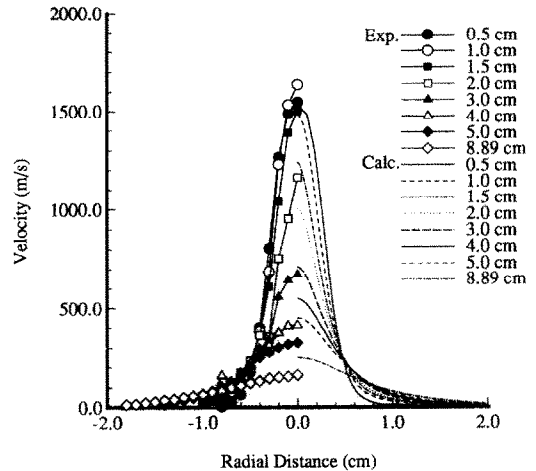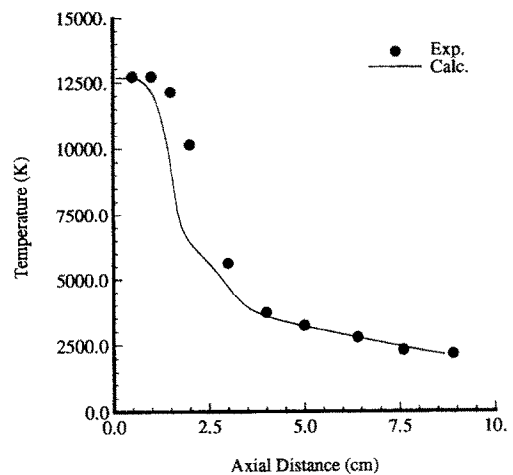

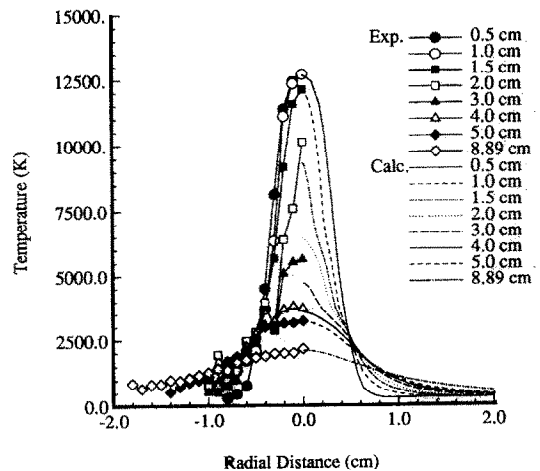FIG. 6. Calculated and experimental temperature along the centerline.

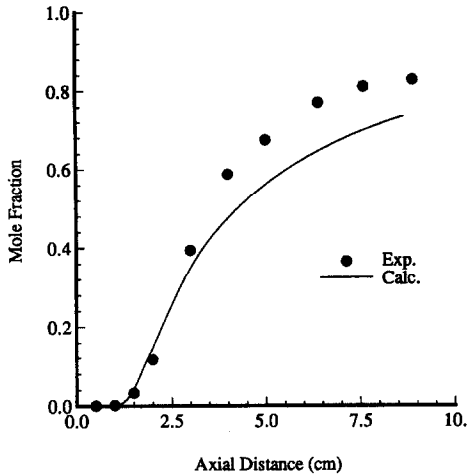FIG. 7. Calculated and experimental radial temperature profiles.

FIG. 8. Calculated and experimental air cold mole fraction along the centerline.

and uncertain inflow profiles of turbulence at the nozzle exit plane.

The cold mole fraction of air is shown in Figs. 8 and 9. Air fraction is used as a measure of the entrainment of surrounding gas. For the turbulent mixing layer examined here diffusive separation of nitrogen and oxygen was not observed, hence the N_2/O_2 ratio is constant. The steep increase of entrained air in Fig. 8 corresponds to the sharp decrease in the axial velocity in Fig. 4 and temperature in Fig. 6. There is a noticeable change in the slope in both Figs. 4 and 6 at approximately 1.0 cm corresponding to the point at which the mixing layer reaches the jet centerline and the concentration of air in the core region becomes significant. In the periphery of the jet, near the torch exit, the radial gradients of axial velocity, temperature, and air cold mole fraction are very steep, as shown in Figs. 5, 7, and 9. As the external atmosphere is entrained, the jet slows and spreads and the profiles flatten. This entrainment and mixing process is more or less complete at 4.0 cm also corresponding with a
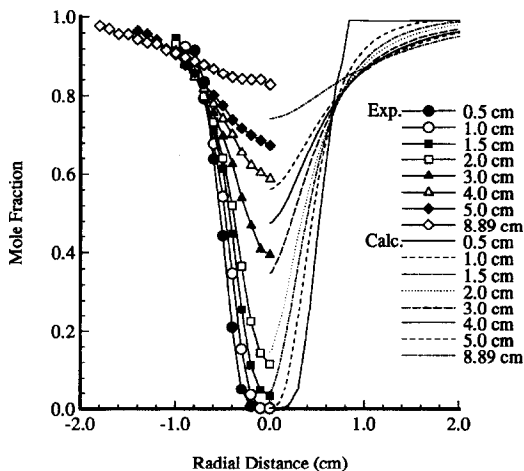

FIG. 9. Calculated and experimental radial profiles of air cold mole fraction.

noticeable change in slope in the velocity and temperature curves. At this point the mixing process has flattened the radial gradients and spread the flow field, Fig. 10, to the point that the rate of decay in velocity and temperature is greatly decreased.

The centerline argon/helium cold mole fraction ratio, Fig. 11, is approximately 1.2 at the 0.5 cm axial location as compared to 2.4 for the premixed plasma gas. Between 0.5 and 1.0 cm the ratio continues to decrease due to diffusive demixing. Figure 12 shows Ar-He cold mole fraction ratio versus radial position for axial locations of 0.5 (inflow), 2.0 and 5.0 cm. In the periphery of the jet the experimentally measured ratio is 2.6, slightly elevated over the premixed value. Calculated results show more mixing, consistent with the overly diffusive characteristic discussed above. After the shear layer surrounding the jet has reached the centerline (the 1.0 cm axial location), turbulent mixing overcomes diffusive demixing and the Ar–He ratio increases. At 5.0 cm the profile of Ar–He mole fraction ratio has been flattened by the mixing process and is approaching a ratio of 2.0 on the centerline.

The observed enhancement in helium concentration over that of the premixed feed gases by almost a factor of two near the torch exit is driven by diffusive demixing in the discharge region. In the discharge region, due to the differences in ionization potential for argon (15.8 eV) and helium (24.6 eV), the argon is preferentially ionized near the torch centerline where temperatures are highest, creating concentration gradients in both argon ions and electrons. This results in ambipolar diffusion of argon radially outward. In addition, since each ionization event produces two particles from one, the helium mole fraction near the centerline is reduced. This causes helium to diffuse inward, resulting in helium enrichment near the centerline and depletion near the torch wall. The degree of demixing is primarily determined in the discharge. This diffusional separation process continues for some distance downstream of the nozzle exit. Eventually, however, recombination occurs as temperatures drop and the argon and helium remix, approaching the initial mixture ratio.

The calculated results show the same trends and reproduce the observed continuation of demixing, Fig. 11. Previous simplified approaches based on cold mole fraction [24, 25] would predict immediate mixing. Hence, it is obvious that complete treatment of multi-component diffusion and ambipolar diffusion is necessary in order to simulate this diffusive demixing process.

CONCLUSIONS

The enthalpy probe is a robust tool for studying thermal plasmas. Complete maps of the gas flow field including velocity, temperature and species concentration, are made with relative ease and expediency by automation of both data acquisition and sequence/position control. The enthalpy, temperature, and vel-
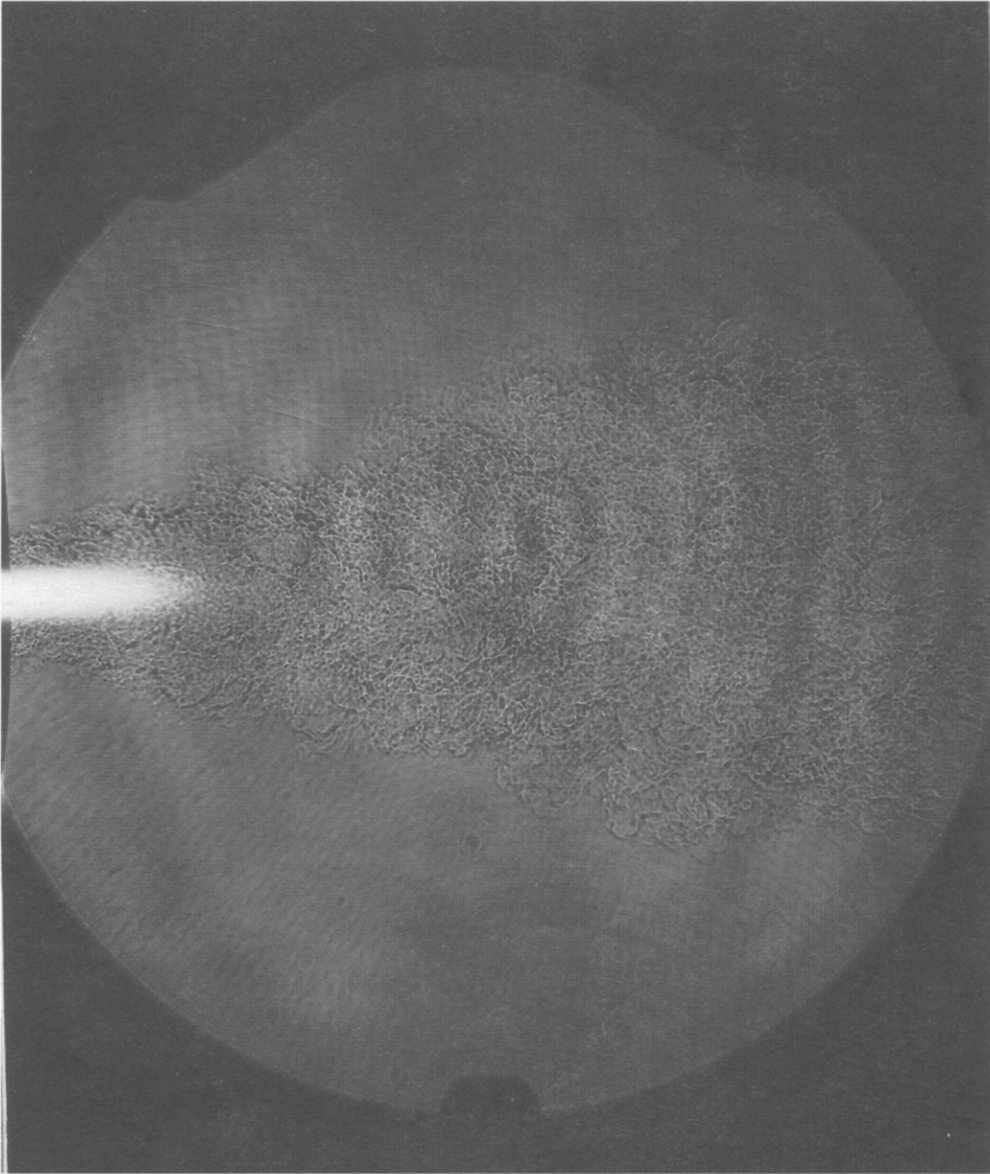
FIG. 10. Pulsed Schlieren of plasma flow field. For reference the circular image is 75 mm in diameter.

ocity obtained all depend on an accurate calculation of the thermodynamic properties of the gas mixture. Accurate properties in turn depend on an accurate measurement of the gas composition. Incorporating a mass spectrometer with the enthalpy probe system provides a quantitative measurement of the gas constituents. This yields valuable information on entrainment, demixing, diffusion, and chemical reactions taking place in thermal plasmas.

The numerical simulation of the Ar–He plasma jet discharging into cold air demonstrated the capabilities of our general multicomponent ambipolar diffusion algorithm by a successful simulation of further demixing of Ar and He in the downstream region of the nozzle exit and re-mixing processes at the far downstream region. Interactions of all ionization reactions

have also been treated in a general and fully self-consistent manner. In this numerical simulation, however, experimentally determined inflow profiles were used as boundary conditions due to the lack of models capable of predicting multicomponent plasma flow inside the plasma torch in a fully self-consistent manner. Complete experimental determination of all the necessary inflow conditions including radial velocity and turbulence was not possible. Hence, it is necessary to assume profiles of radial velocity and turbulence.

We suspect that inadequacies in the turbulence model are among the most significant source of errors. The simple k–ε model employed in this study is not really satisfactory even for simple flows, requiring case-by-case ad hoc corrections. It would be rather
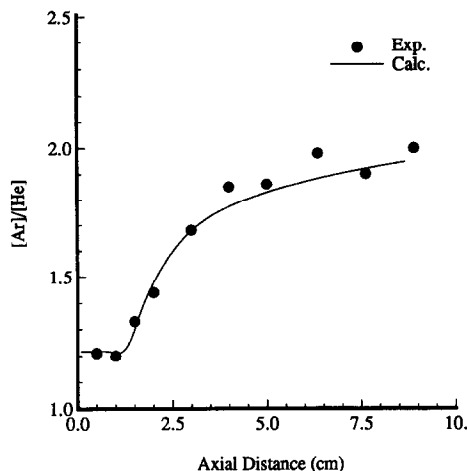
FIG. 11. Calculated and experimental argon to helium cold mole fraction ratio along the centerline.
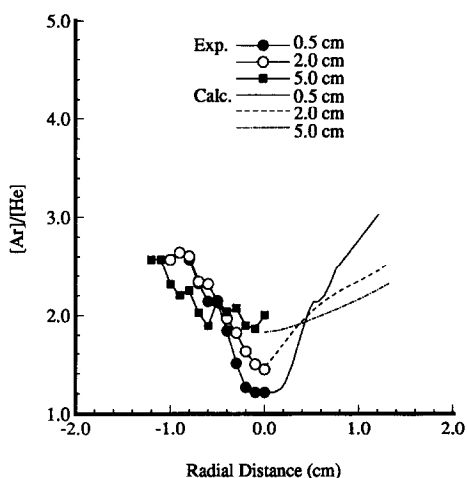

FIG. 12. Calculated and experimental radial profiles of argon to helium cold mole fraction ratio.

remarkable if this model were quantitatively applicable to thermal plasmas without further significant modifications. It appears that more detailed and accurate turbulence models will probably be required to achieve satisfactory accuracy in the simulation of complex plasma flows. However, the present simple model nevertheless yields useful semiquantitative results with fair accuracy. Further research is needed to determine capabilities and applicability of various turbulence models for thermal plasma flows.

REFERENCES

1. E. Pfender, J. R. Fincke and R. Spores, Entrainment of cold gas into thermal plasma jets, *Plasma Chem. Plasma Process.* **11**, 529–542 (1991).
2. J. R. Fincke, R. Rodriguez and C. G. Pentecost, Coher-ent anti-Stokes Raman spectroscopic measurement of air entrainment in argon plasma jets, *Plasma Processing and Synthesis of Materials III, Materials Research Society Symposia Proceedings*, Vol. 190, pp. 184–189, San Francisco, CA (1990).
3. J. R. Fincke, R. Rodriguez and C. G. Pentecost, Measurement of air entrainment in plasma jets, *Proc. 1990 National Thermal Spray Conference*, pp. 45–48, Long Beach, CA (1990).
4. R. Spores and E. Pfender, Flow structure of a turbulent plasma jet, *Proc. 1988 National Thermal Spray Conference*, pp. 85–92, Cincinnati, OH (1988).
5. M. Vardelle, A. Vardelle, P. Roumilhac and P. Fauchais, Influence of the surrounding atmosphere under plasma spraying conditions, *Proc. 1988 National Thermal Spray Conference*, pp. 117–121, Cincinnati, OH (1988).
6. W. Frie and H. Maecker, Massentrennung durch Diffusion reagierender Gase, *Zs. f. Physick, Bd.* **162**, 69–83 (1961).
7. H. Maecker, Fortschritte in der Bogenphysik, *Proc. Fifth Int'l Conf. on Ionization Phen. in Gases*, Vol. 162, pp. 1793–1811. North-Holland, The Netherlands (1961).
8. J. Richter, Über Diffusionsvorgänge in Lichtbögen, *Zs. f. Astrophysik* **53**, 262–272 (1961).
9. W. Frie, Berechnung der Gaszusammensetzung und der Materialfunktionen von SF6, *Zs. f. Physik, Bd.* **201**, 269–294 (1967).
10. D. Vukanovic and V. Vukanovic, On the behavior of hydrogen isotopes in a D.C. arc *Plasma, Spectrochimica Acta* **24B**, 579–583 (1969).
11. G. Baruschka and E. Schulz-Gulde, Transition probabilities for F I Lines from wall stabilized arc measurements, *Astron. Astrophys.* **44**, 335–342 (1975).
12. E. Fisher, Axial segregation of additives in mercury-metal-halide arcs, *J. Appl. Phys.* **47**, 2954–2960 (1976).
13. H.-P. Stormberg, Axial and radial segregation in metal halide arcs, *J. Appl. Phys.* **52**, 3233–3237 (1981).
14. J. Grey, P. F. Jacobs and M. P. Sherman, Calorimetric probe for the measurement of extremely high temperatures, *Rev. Sci. Instrum.* **33**, 738–741 (1962).
15. J. Grey, Sensitivity analysis for the calorimetric probe, *Rev. Sci. Instrum.* **34**, 857–859 (1963).
16. J. Grey, Thermodynamic methods of high-temperature measurement, *ISA Trans.* **4**, 102–115 (1965).
17. S. Katta, J. A. Lewis and W. H. Galvin, A plasma calorimetric probe, *Rev. Sci. Instrum.* **44**, 1519–1523 (1973).
18. W. L. T. Chen, J. Heberlein and E. Pfender, Experimental measurements of plasma properties for Miller SG-100 Torch with Mach I settings. Part 1. Enthalpy probe measurements, Report, Engineering Research Center for Plasma-Aided Manufacturing, Department of Mechanical Engineering, University of Minnesota (1990).
19. M. Brossa and E. Pfender, Probe measurements in thermal plasma jets, *Plasma Chem. Plasma Process.* **8**, 75–90 (1988).
20. A. Capetti and E. Pfender, Probe measurements in argon plasma jets operated in ambient argon, *Plasma Chem. Plasma Process.* **9**, 329–339 (1989).
21. P. Stefanovic, P. Pavlovic and M. Jankovic, High sensitive calorimetric probe for diagnostics thermal plasma at the exit of electric arc heater, *Proc. 9th Int. Symp. Plasma Chemistry (ISPC-9)*, Vol. 1, pp. 117–121, Pugnochiuso, Italy (1989).
22. W. D. Swank, J. R. Fincke and D. C. Haggard, Modular enthalpy probe and gas analyzer for thermal plasma measurements, *Rev. Sci. Instrum.* **64**, 56–62 (1993).
23. J. R. Fincke, S. C. Snyder and W. D. Swank, Comparison of enthalpy probe and laser light scattering measurement of thermal plasma temperatures and velocities, *Rev. Sci. Instrum.* **64**, 711–724 (1993).
24. Y. P. Chyou and E. Pfender, Modeling of plasma jets

with superimposed vortex flow, *Plasma Chem. Plasma Process.* **9**, 291–328 (1989).

25. A. H. Dilawari, J. Szekely and R. Westhoff, A comparison of experimental measurements and theoretical predictions regarding the behavior of a turbulent argon plasma jet discharging into air, *Plasma Chem. Plasma Process.* **10**, 501–513 (1990).

26. M. Mitchner and C. H. Kruger, *Partially Ionized Gases*, p. 146. Wiley, New York (1973).

27. J. D. Ramshaw and C. H. Chang, Ambipolar diffusion in multicomponent plasmas, *Plasma Chem. Plasma Process.* **11**, 395–402 (1991).

28. J. D. Ramshaw, Self-consistent effective binary diffusion in multicomponent gas mixtures, *J. Non-equilib. Thermodyn.* **15**, 295–300 (1990).

29. J. D. Ramshaw and C. H. Chang, Computational fluid dynamics modeling of multicomponent thermal plasmas, *Plasma Chem. Plasma Process.* **12**, 299–325 (1992).

30. C. H. Chang and J. D. Ramshaw, Numerical simulations of argon plasma jets flowing into cold air, *Plasma Chem. Plasma Process.* **13**, 189–209 (1993).

31. C. H. Chang, Numerical simulation of alumina spraying in an argon–helium plasma jet, *Proc. International Thermal Spray Conference (ITSC'92)*, pp. 793–798, Orlando, FL (1992).

32. B. Pateyron, M.-F. Elchinger, G. Delluc and P. Fauchais, Thermodynamic and transport properties of Ar–H_2 and Ar–He plasma gases used for spraying at atmospheric pressure, I. Properties of the mixtures, *Plasma Chem. Plasma Process.* **12**, 421–448 (1992).

33. E. Pfender, Private communication (1989).

34. B. E. Launder, A. Morse, W. Rodi and D. B. Spalding, The prediction of free shear flow—A comparison of the performance of six turbulence models. NASA SP-321 (1972).

35. M. A. Leschziner and W. Rodi, Computation of strongly swirling axisymmetric free jets. *AIAA J.* **22**, 1742–1747 (1984).